34th Annual International Conference of the IEEE EMBS
San Diego, California USA, 28 August - 1 September, 2012

Computational Modeling of the Transient Hemodynamic Response in Cerebral Cortex*

Jung Hwan Kim, Reswanul K. Khan, David Ress

Abstract— **Neural activity triggers a vascular response in the brain that leads to transient changes in oxygen transport, and this mechanism is the basis for popular and powerful functional imaging methods. However, there is limited understanding of oxygen delivery to cerebral cortex both in steady state and during transient perturbations. In this study, a computational model for oxygen transport in the brain was developed and used to fit polarographic oxygen measurements during transient stimulation in cerebral cortex. The hemodynamic response function (HRF) was modeled with convection-diffusion transport in a four-compartment system (erythrocyte, intravascular, extravascular, and intracellular) that includes oxygen dissociation from hemoglobin. This model explained the dynamics of oxygen transport in cortex after brief visual stimulation, successfully fitting ~90% of experimental measurements within a realistic range of parameters for steady-state flow speed and oxygen consumption, as well as flow and oxygen uptake perturbations.**

1. Introduction

A detailed understanding of oxygen transport in the brain is of critical value to science and medicine. The utility of hemodynamic imaging techniques such as fMRI highlights the need for better understanding of neurovascular coupling. In brain imaging experiments, use is made of the hemodynamic response function (HRF), the vascular response evoked by brief (few sec) neural activation. In tissue, the HRF exhibits a variety of oscillatory forms that are associated with changes in oxygen uptake and blood flow. Because the brain is continually active, it is likely that such transient hemodynamic responses occur continually.

Oxygen transport in the brain is poorly understood, with even steady-state transport in controversy. In particular, it is not clear what role arterioles play in cortical oxygen transport to the tissue. In cerebral cortex, oxygen transport seems to occur predominantly in small cortical arterioles and capillaries [1-3]. In non-brain tissues, however, arterioles seem to play a dominant role in oxygen transport, with less transfer via the capillaries[4, 5]. Moreover, oxygen diffusion from arterioles and capillaries appears to be insufficient to explain total oxygen loss [6, 7]. Based on such measurements, it has been suggested that in non-brain tissues, the missing oxygen is consumed by endothelial cells of the vascular wall [5, 8]. In the brain, however, such a mechanism remains controversial, as it has not been confirmed by measurements [1, 9].

*Research supported by NIH National Heart, Lung, and Blood Institute.

Jung Hwan Kim and David Ress are with the Section of Neurobiology and Imaging Research Center, The University of Texas, Austin, TX 78759 USA (phone: 512-232-5270; e-mail: ress@mail.utexas.edu)

Reswanul K. Khan is with the Department of Physics, in addition to the previous affiliations at The University of Texas at Austin.

A number of models have been proposed for the dynamics of the HRF, particularly as it is manifest by hemodynamic brain imaging methods. The "balloon model" has been the most popular [10, 11]. It explains the HRF based on volume changes in intra- and extravascular compartments with non-linear compliance. The volume changes were postulated to occur in venules and veins, as the global compliance of venous system is known to be substantial [12, 13]. A similar form for this model utilizes a lumped-element network analogy that includes a non-linear compliant element [14, 15]. Such models have become increasingly sophisticated and complex [16-18]. However, recent experiments have not shown much local venular dilation in the brain for brief periods of stimulation (< 10 sec); volume increases seem mostly to occur on the arterial side of the system [2, 19, 20]. Accordingly, there is a need to revisit theoretical models for the HRF.

In order to understand the healthy operation of the brain, and the mechanisms of hemodynamic imaging, we need to better understand the processes that give rise to the HRF. In our previous study, we proposed use of a lumped linear equivalent-circuit model for the blood flow dynamics in the pial arterioles, the four-element windkessel (FEW). A convection-diffusion transport model was developed within a three-compartment (intra- and extravascular, intracellular) system [21]. The model provided detailed fits to a large ensemble of locally resolved measurements of relative tissue oxygen changes during transient stimulation. Here, we expand the model to include the dynamics of hemoglobin oxygen dissociation, thereby improving predictions of intravascular oxygen concentration. The inclusion of dissociation also enables absolute rather than relative predictions of both steady state and transient hemodynamic quantities. The results are in broad agreement with the same set of experimental measurements. The expanded model provides a simple but remarkably effective description of a range of hemodynamic transport phenomena in the complex vascular geometry of the mammalian brain.

2. Materials and Methods

A. Oxygen Transport Model

A one-dimensional cylindrical geometry was employed (Fig. 1). The inner two compartments, erythrocyte and plasma, represented blood flow that provided convective oxygen input. Flow speed is given by $U(t) = U_0 + U_1(t)$, a combination of steady flow and a time-varying perturbation that we modeled using the FEW (Fig. 2). An artificial flux term, $F(z, t)$, was introduced for oxygen dissociation from the erythrocytes into the plasma. The outer two compartments, extravascular and intracellular, represented the static tissue. Diffusion coupled the plasma oxygen to the extracellular compartment, while the intracellular compartment serves

only as a sink for cerebral metabolism of oxygen ($CMRO_2$), $\Gamma(t) = \Gamma_0 + \Gamma_1(t)$, also assumed to consist of a steady-state component and a perturbation term driven by the neural stimulation transient.

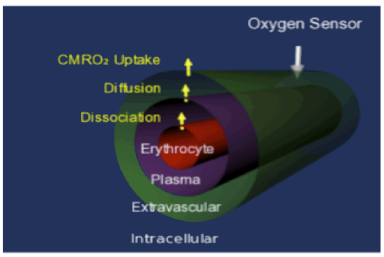

Figure 1. Schematic diagram of the four-compartment model

In the FEW (Fig. 2), the inertive element, I, modeled Newton's 2nd law for blood flow in the pial arteries; inertia must be included where the Reynolds number is >1, e.g. large arterioles. The series resistance, $R_1 = R_{1a} + R_{1b}$, represented frictional losses associated with the parallel combination of all downstream flow through the fractal vascular tree. The combination of element C and resistance R_2, represented the compliance of the downstream venous vasculature. In steady state, neglecting pulsatility, there is constant pressure at point **T**, which represented the input to the model. We assumed that the intravascular cylinder coupled resistively to the larger network, but the load resistance R_A was much greater than R_1 and R_2, so that it did not perturb the global dynamics. The transient behavior of this system was modeled by the switch across R_{1b}, which briefly closed to simulate a vasodilation that decreased the upstream vascular resistance. Because there was steady-state flow through I, the vasodilation created a brief positive pressure fluctuation at **T**, which was described by the impulse response of the network, eqn. (1).

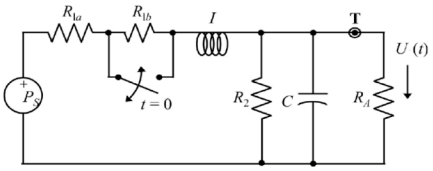

Figure 2. Linear network for the four-element windkessel

The impulse response of this linear system characterized its behavior, which had two forms depending upon the time constants of the system: underdamped and overdamped. The flow perturbation was thus specified by three parameters: frequency f, time constant τ, and amplitude U_{10}. Most experimental fits indicated an under-damped response.

$$U_1(t) = U_{10}\begin{cases}\exp(-t/\tau)\sin(2\pi ft) & \text{underdamped}\\ \exp(-t/\tau)\sin(2uft) & \text{overdamped}\end{cases} \quad (1)$$

We used convection-diffusion equations to describe transport in erythrocyte (2), plasma/intravascular (3), and extravascular (4) compartments:

$$\frac{\partial Q_b}{\partial t} = -\frac{F(z,t)}{C_b} - U(t)\frac{\partial Q_b}{\partial z} \quad (2)$$

$$\frac{\partial Q_p}{\partial t} = \frac{F(z,t)}{C_p} - A(Q_p - Q_e) - U(t)\frac{\partial Q_p}{\partial z} \quad (3)$$

$$\frac{\partial Q_e}{\partial t} = A\frac{C_p}{C_e}(Q_p - Q_e) - \frac{C_b + C_p}{cC_e}\Gamma(t) \quad (4)$$

where oxygen concentration is Q, effective cerebral blood volume (CBV) fraction is c, intravascular velocity is $U(t)$, $CMRO_2$ from the intracellular space is $\Gamma(t)$. The artificial flux $F(z, t)$ represented oxygen transport from erythrocyte to plasma. The diffusion rate constant, A, is the diffusivity weighted by the lineal surface–to-volume ratio of the intravascular compartment. Volume per unit length is C, subscripts b, p, and e represent erythrocyte, plasma and extravascular compartments, respectively. Extravascular volume changes corresponding to transient perturbations are neglected.

The Hill equation gives a non-linear description of oxygen dissociation from hemoglobin that relates Q_b and Q_p. However, dissociation in the cerebral microvasculature can be assumed approximately linear because of its fairly narrow range of oxygen saturation. We therefore used a piecewise linear approximation:

$$Q_b(\text{mmol/L}) = \begin{cases}0 & (Q_p < 0.09 \text{ mmol/L})\\ \kappa Q_p + q_0 & \\ 9.2 & (Q_p > 0.64 \text{ mmol/L})\end{cases} \quad (5)$$

$$\kappa \cong 118,\ q_0 \cong -0.61$$

B. Modeling tissue-oxygen measurements

The new model was used to fit a large set of experimental measurements of transient tissue oxygen responses in cat visual cortex obtained for a oriented grating stimuli that were presented for 4-s periods [22]. We allowed five parameters to vary in fitting each measurement time course: $CMRO_2$ perturbation amplitude Γ_{10}, flow perturbation amplitude U_{10}, frequency f, and damping time τ. and cylinder length L. Initial conditions for modeling the experimental measurements were first obtained from the steady state solution of (2)—(4). We then evolved these equations for the period of the measurement (30 s), to provide a prediction.

The stimulation-induced $CMRO_2$ perturbation $\Gamma_1(t)$ was modeled as a rectangle-function increase with amplitude Γ_{10}. The experimental flow response was simulated by the convolution of the FEW impulse response (Eqn. 3) with a 4-s rectangular pulse corresponding to the visual stimulation.

Steady-state solution of (2)—(4) yielded the following relationships that link the cylinder length parameter, L, to steady-state $CMRO_2$ and oxygen diffusion rate:

$$\Gamma_0 = \frac{EU_0 Q_{p00} c\left[\nu\kappa + (1-\nu)\right]}{L} \quad (6)$$

$$A = \frac{EU_0\left[\nu\kappa + (1-\nu)\right]}{\sigma L(1-\nu)}, \quad (7)$$

where hematocrit is ν, oxygen extraction fraction is E. The oxygen concentration boundary condition at the upstream end of the cylinder is Q_{p00}, which was calculated based on the measured oxygen saturation in 3rd-order arterioles [3]. From this, we obtained $Q_{e00} = (1 - \sigma)Q_{p00}$, where σ was the transmural gradient at the upstream end of the cylinder. We chose a $\sigma = 0.1$ to obtain good fits. The downstream plasma concentration was $Q_{p0}(L) = (1 - E)Q_{p00}$. Thus, the choice of L

sets Γ_0 and A, permitting the evolution of (2)—(4) with a given parameter set.

We assumed that only a fraction of the parenchymal blood volume participates in oxygen transport; blood contained in larger arterioles and venules is generally included in the CBV but probably does not contribute significantly to oxygen transfer. We therefore defined and utilized an effective CBV that includes contributions from only the small arterioles (<30 μm diameter) and capillaries by weighting their compartmental volume fractions [23] by their experimentally estimated oxygen transport contributions [3, 5] to obtain c ≈ 0.017 (29% of CBV). Oxygen extraction fraction E was set to 0.44 [3, 5, 24]; hematocrit v was set to 0.35 [25, 26]. Flow speed U_0 = 1.84 mm/s was chosen based upon experimental findings [3] together with a weighting procedure similar to that used for the calculation of c.

We then allowed the five fitting parameters L, Γ_{10}, f, τ, and U_{10}, to vary in the course of a non-linear optimization that sought to minimize the error between prediction and measurement in a maximum likelihood sense. Best-fit parameters were obtained by minimizing the negative sum of the log-likelihood of the model at all time points, given the data. The quality of a fit was assessed by computing the mean deviation between the fit of the measurement as a fraction of the experimental standard error. Fits where the mean deviation was <1 were considered successful.

3. Results

Most fits exhibited an initial oxygen decrease in extravascular compartment caused by the oxygen uptake perturbation. Subsequently, there was often a positive phase of oxygen increase produced by the flow perturbation, which overwhelmed the extravascular oxygen demand. Later, an undershoot was produced by the flow perturbation, with late-time oscillation back to the baseline level, Fig. 3A. The extended model was also capable of fitting a wide gamut of variations in the measured HRF. For example, some of measurements were dominated by a strong flow perturbation: more "ringing" in Fig. 3A and 3B compared with relatively modest "ringing" in Fig. 3C and 3D. Some measurements also showed larger early transient oxygen uptake, Fig. 3B and 3D, and less flow perturbation, Fig. 3D.

The model successfully fit ~90% of the experimental measurements. Experimental measurements for the unsuccessful fits had qualitatively unusual dynamics such as multiple or delayed initial dip(s), or oxygen levels not returning to baseline at the end of the measurement.

Table I provides mean and standard deviation values for each parameter across the 166 experimental measurements. $CMRO_2$ changes were ~10 %, which is similar to the value observed using PET [24]. Resting $CMRO_2$ was 0.015 mmol/L/s, in good agreement with measurements of 0.006—0.058 [27]. However, mean diffusion rate A was 140/s, 3× lower than calculated from the literature [3, 29].

Mean length was 5.7 mm, much longer than the 0.7 mm obtained with our earlier model [21]. Frequency f was ~0.09 Hz, similar to our previous results. Damping time τ was again long, ~17 s, reflecting the often strongly underdamped character of the measured response. However, a minority of the measurements were more damped, e.g., Fig. 3C; τ exhibited large variability. Flow perturbations were substantial, ~13%, but also strongly variable, with measurements showing a wide range of perturbations, e.g., Fig. 3D shows a small flow perturbation, while Figs. 3A, C show large perturbations. $CMRO_2$ perturbations were similarly substantial, ~9%, much larger than predicted by our previous model.

TABLE I. Mean and Standard Deviation (STD) of Steady-State and Perturbation Parameters.

	Steady-state parameters				
	Quality (%)	**Γ_0 (mmol/L-s)**			**A (s^{-1})**
Mean	89.8	0.015			139.7
STD	N/A	0.010			94.3
	Perturbation parameters				
	L (mm)	**f (Hz)**	**τ (s)**	**U_1/U_0 (%)**	**Γ_1/Γ_0 (%)**
Mean	5.7	0.087	17.4	13.0	9.5
STD	2.5	0.023	15.9	8.2	4.0

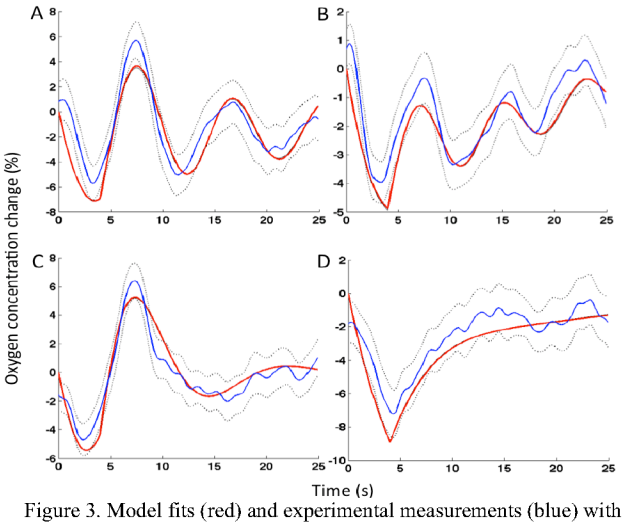

Figure 3. Model fits (red) and experimental measurements (blue) with standard error (surrounding dotted lines)

4. Discussion

Our expanded model adopts the philosophy of representing the oxygen-transport components of the fractal vascular network in a concentric cylindrical geometry of adjustable length. The model can be viewed as representing a single, stereotypical element of this network, a "vascular unit" starting with a pial penetrating arteriole through its associated capillary beds. Oxygen transport in this unit is calculated directly by a convection-diffusion model, while flow processes are assumed to be mediated outside the oxygen-transport region as described by the FEW linear network. Using this model, HRF responses with highly heterogeneous combinations of three phases – initial dip or latency, hyperoxic peak, and undershoot followed by oscillation – were accurately modeled with only five perturbation parameters.

The model provided accurate fits using realistic estimates for flow speeds, effective CBV, upstream hemoglobin oxygen concentration, hematocrit, and extraction fraction. Both flow and $CMRO_2$ perturbations were well quantified by

the model, compared to the literature [3, 5, 24-26].

There were also some parameter disagreements. Mean length was 5.7 mm, much longer than the suggested value, 0.9 mm, for oxygen transport from small arterioles to capillaries [3, 17, 28]. Moreover, the model used a diffusion constant (A) that was ~3× lower than would be inferred from the literature [3, 29]. Finally, to obtain good fits, we had to use a small value for the upstream transmural oxygen gradient, $\sigma = 0.1$, while reported estimates range from 0.2—0.34 [5, 8]. It is likely that our simple geometry does not provide a realistic description of the transport dynamics; by representing the vastly branching capillary bed by a single cylinder, we underestimate the surface-area-to-volume ratio. We could remediate this flaw by using a parallel network that breaks the effective blood volume into many identical branches. Also, we could possibly explain larger transmural gradients by making use of a previously proposed wall-loss mechanism [5, 8]. Another limitation in our current modeling is the error associating with a piecewise linear approximation for Hill equation, which could have underestimated oxygen transport between both plasma and erythrocyte compartments resulting in a longer cylinder length. This limitation could be rectified by using a first-order Taylor expansion of the Hill equation.

ACKNOWLEDGMENT

We thank Jeff Thompson and Ralph Freeman for their assistance in providing and interpreting the experimental data in this paper. Research supported by R21HL108143.

References

[1] M. Sharan, E. P. Vovenko, A. Vadapalli, A. S. Popel, and R. N. Pittman, "Experimental and theoretical studies of oxygen gradients in rat pial microvessels," *J. Cereb. Blood Flow Metab.,* vol. 28, pp. 1597-1604, Sep 2008.

[2] A. L. Vazquez, M. Fukuda, M. L. Tasker, K. Masamoto, and S. G. Kim, "Changes in cerebral arterial, tissue and venous oxygenation with evoked neural stimulation: implications for hemoglobin-based functional neuroimaging," *J. Cereb. Blood Flow Metab.,* vol. 30, pp. 428-439, Feb 2010.

[3] E. Vovenko, "Distribution of oxygen tension on the surface of arterioles, capillaries and venules of brain cortex and in tissue in normoxia: an experimental study on rats," *Pflug. Arch. Eur. J. Phy.,* vol. 437, pp. 617-623, Mar 1999.

[4] I. P. Torres, H. Kerger, and M. Intaglietta, "PO(2) measurements in arteriolar networks," *Microvasc. Res.,* vol. 51, pp. 202-212, Mar 1996.

[5] A. G. Tsai, P. C. Johnson, and M. Intaglietta, "Oxygen gradients in the microcirculation," *Physiol. Rev.,* vol. 83, pp. 933-963, Jul 2003.

[6] M. Intaglietta, P. C. Johnson, and R. M. Winslow, "Microvascular and tissue oxygen distribution," *Cardiovasc. Res.,* vol. 32, pp. 632-643, Oct 1996.

[7] A. S. Popel, R. N. Pittman, and M. L. Ellsworth, "Rate of oxygen loss from arterioles is an order of magnitude higher than expected," *Am. J. Physiol.,* vol. 256, pp. H921-H924, Mar 1989.

[8] A. G. Tsai, B. Friesenecker, M. C. Mazzoni, H. Kerger, D. G. Buerk, P. C. Johnson, and M. Intaglietta, "Microvascular and tissue oxygen gradients in the rat mesentery," *Proc. Natl. Acad. Sci. U. S. A.,* vol. 95, pp. 6590-6595, Jun 1998.

[9] E. P. Vovenko, "Transmural oxygen tension gradients in rat cerebral cortex arterioles," *Neurosci. Behav. Physiol.,* vol. 39, pp. 363-70, 2009-May 2009.

[10] R. B. Buxton, K. Uludag, D. J. Dubowitz, and T. T. Liu, "Modeling the hemodynamic response to brain activation," *Neuroimage,* vol. 23, pp. S220-S233, 2004.

[11] R. B. Buxton, E. C. Wong, and L. R. Frank, "Dynamics of blood flow and oxygenation changes during brain activation: The balloon model," *Magn. Reson. Med.,* vol. 39, pp. 855-864, Jun 1998.

[12] T. Binzoni, V. Quaresima, M. Ferrari, E. Hiltbrand, and P. Cerretelli, "Human calf microvascular compliance measured by near-infrared spectroscopy," *J. Appl. Physiol.,* vol. 88, pp. 369-372, Feb 2000.

[13] J. S. Romney and R. Z. Lewanczuk, "Vascular compliance is reduced in the early stages of type 1 diabetes," *Diabetes Care,* vol. 24, pp. 2102-2106, Dec 2001.

[14] K. J. Friston, A. Mechelli, R. Turner, and C. J. Price, "Nonlinear responses in fMRI: The balloon model, volterra kernels, and other hemodynamics," *Neuroimage,* vol. 12, pp. 466-477, Oct 2000.

[15] J. B. Mandeville, J. J. A. Marota, C. Ayata, G. Zaharchuk, M. A. Moskowitz, B. R. Rosen, and R. M. Weisskoff, "Evidence of a cerebrovascular postarteriole windkessel with delayed compliance," *J. Cereb. Blood Flow Metab.,* vol. 19, pp. 679-689, Jun 1999.

[16] T. J. Huppert, M. S. Allen, H. Benav, P. B. Jones, and D. A. Boas, "A multicompartment vascular model for inferring baseline and functional changes in cerebral oxygen metabolism and arterial dilation," *J. Cereb. Blood Flow Metab.,* vol. 27, pp. 1262-1279, Jun 2007.

[17] Y. Zheng, D. Johnston, J. Berwick, D. M. Chen, S. Billings, and J. Mayhew, "A three-compartment model of the hemodynamic response and oxygen delivery to brain," *Neuroimage,* vol. 28, pp. 925-939, Dec 2005.

[18] Y. Zheng, J. Martindale, D. Johnston, M. Jones, J. Berwick, and J. Mayhew, "A model of the Hemodynamic response and oxygen delivery to brain," *Neuroimage,* vol. 16, pp. 617-637, Jul 2002.

[19] A. Devor, S. Sakadzic, P. A. Saisan, M. A. Yaseen, E. Roussakis, V. J. Srinivasan, S. A. Vinogradov, B. R. Rosen, R. B. Buxton, A. M. Dale, and D. A. Boas, ""Overshoot" of O(2) Is Required to Maintain Baseline Tissue Oxygenation at Locations Distal to Blood Vessels," *J. Neurosci.,* vol. 31, pp. 13676-13681, Sep 2011.

[20] T. Kim, K. S. Hendrich, K. Masamoto, and S. G. Kim, "Arterial versus total blood volume changes during neural activity-induced cerebral blood flow change: implication for BOLD fMRI," *J. Cereb. Blood Flow Metab.,* vol. 27, pp. 1235-1247, Jun 2007.

[21] D. Ress, J. K. Thompson, B. Rokers, R. Khan, and A. C. Huk, "A model for transient oxygen delivery in cerebral cortex," *Front Neuroenergetics,* vol. 1, p. 3, Jun 2009.

[22] J. K. Thompson, M. R. Peterson, and R. D. Freeman, "Single-neuron activity and tissue oxygenation in the cerebral cortex," *Science,* vol. 299, pp. 1070-1072, Feb 2003.

[23] F. Cassot, F. Lauwers, C. Fouard, S. Prohaska, and V. Lauwers-Cances, "A novel three-dimensional computer-assisted method for a quantitative study of microvascular networks of the human cerebral cortex," *Microcirculation,* vol. 13, pp. 1-18, Jan-Feb 2006.

[24] H. Ito, I. Kanno, C. Kato, T. Sasaki, K. Ishii, Y. Ouchi, A. Iida, H. Okazawa, K. Hayashida, N. Tsuyuguchi, Y. Kuwabara, and M. Senda, "Database of normal human cerebral blood flow, cerebral blood volume, cerebral oxygen extraction fraction and cerebral metabolic rate of oxygen measured by positron emission tomography with O-15-labelled carbon dioxide or water, carbon monoxide and oxygen: a multicentre study in Japan," *Eur. J. Nucl. Med. Mol. Imaging,* vol. 31, pp. 635-643, May 2004.

[25] H. H. Lipowsky, "Microvascular rheology and hemodynamics," *Microcirculation,* vol. 12, pp. 5-15, Jan-Feb 2005.

[26] J. A. Ulatowski, E. Bucci, A. Razynska, R. J. Traystman, and R. C. Koehler, "Cerebral blood flow during hypoxic hypoxia with plasma-based hemoglobin at reduced hematocrit," *Am. J. Physiol-Heart C,* vol. 274, pp. H1933-H1942, Jun 1998.

[27] E. Lenigerfollert, "Direct determination of local oxygen-consumption of brain cortex invivo," *Pflug. Arch. Eur. J. Phy.,* vol. 372, pp. 175-179, 1977.

[28] M. Sharan, M. P. Singh, and A. Aminataei, "A mathematical-model for the computation of the oxygen dissociation curve in human-blood," *Biosystems,* vol. 22, pp. 249-260, 1989.

[29] M. A. Mintun, B. N. Lundstrom, A. Z. Snyder, A. G. Vlassenko, G. L. Shulman, and M. E. Raichle, "Blood flow and oxygen delivery to human brain during functional activity: Theoretical modeling and experimental data," *Proc. Natl. Acad. Sci. U. S. A.,* vol. 98, pp. 6859-6864, Jun 2001.